RSC Advances

PAPER

View Article Online
View Journal | View Issue

Cite this: *RSC Adv.*, 2022, **12**, 35543

Fabrication of photo-Fenton self-cleaning PVDF composite membrane for highly efficient oil-in-water emulsion separation

Chengcai Li,[ab] Minghui Shi,[a] Dan Xu,[a] Qiqi Liao,[a] Guojin Liu,[ac] Yuhai Guo,[ab] Hang Zhang[d] and Hailin Zhu *[ab]

Received 9th November 2022
Accepted 1st December 2022

DOI: 10.1039/d2ra07116a

rsc.li/rsc-advances

The anti-fouling performance of membranes is an important performance in the separation of oil/water. However, the membrane with anti-fouling performance will also have surface scaling phenomenon when it runs for a long time. Therefore, there is still a great demand for stain-resistant membranes with good self-cleaning ability and high flux recovery rate. Based on this, this paper firstly prepared a hydrophilic membrane with carboxyl group and carboxyl ion by blending poly(ethylene-*alt*-maleic anhydride) (PEMA) and polyvinylidene fluoride (PVDF), and then prepared a self-cleaning composite membrane by *in situ* mineralization of β-FeOOH particles on the surface of the membrane for efficient oil-in-water emulsion separation. A large number of $-COOH/COO^-$ and β-FeOOH particles on the membrane surface make the composite membrane have strong hydrophilic properties (WCA = 20.34°) and underwater superoleophobicity (UOCA = 155.10°). These composite membranes have high separation efficiency (98.8%) and high flux (694.56 L m^{-2} h^{-1} bar^{-1}) for soybean oil-in-water emulsion. Importantly, the as-prepared membrane shows excellent flux recovery rate (over 99.93%) attributed to the robust photo-Fenton catalytic activity of β-FeOOH, and the β-FeOOH is chemically bonded to the as-prepared membrane, which makes the as-prepared membrane have good reusability. This work provides hope for the application of self-cleaning membranes in the construction of anti-fouling membranes for wastewater remediation.

1. Introduction

Water pollution has become a major obstacle to economic development, and more and more people are beginning to pay attention to water pollution.[1–5] The increase in oily sewage caused by common petrochemical discharges, domestic wastewater and frequent industrial spills have brought many adverse effects on the aquatic environment and human life.[6–11] At present, oil–water separation is still considered as a worldwide problem. There are many ways to solve the problem of oil pollution, such as adsorption method, centrifugal method, *in situ* combustion method, and so on. These traditional methods all have the problem of secondary pollution, complex operation process and low separation efficiency.[12,13] The membrane separation technology is also one of the most common methods in oil–water separation. Polymer membrane, one of the main membrane materials, has been widely used in water pollution treatment,[14–16] due to its good mechanical properties and easy processing. Microfiltration membranes are widely employed in green wastewater regeneration because of their low energy consumption and high inhibition rate. However, membrane contamination remains one of the main obstacles to the further sustainable development of membrane technology, as microscopic interactions between polymer membrane surfaces and organic contaminants lead to membrane contamination, resulting in reduced separation performance and reduced membrane life.[17,18] Therefore, it is very desirable to develop membranes with excellent stain resistance, but it is challenging to meet the growing environmental requirements. The preparation of microfiltration membranes with high anti-fouling properties is a major method of solving membrane contamination.

At present, there are many methods used to prepare anti-fouling membranes, such as surface crosslinking, coating, surface mineralization, *in situ* blending and other methods, people have made great efforts to design anti-fouling membranes.[19–23] Among them, *in situ* blending features simultaneous membrane formation and modification by one-step method, and shows the advantages of three-dimensional

[a]*Zhejiang Provincial Key Laboratory of Fiber Materials and Manufacturing Technology, Zhejiang Sci-Tech University, Hangzhou, 310018, China. E-mail: zhhailin@163.com*

[b]*Zhejiang Sci-Tech University Huzhou Research Institute Co., Ltd, Huzhou 313000, China*

[c]*Zhejiang Provincial Innovation Center of Advanced Textile Technology, Shaoxing, 312000, China*

[d]*Zhejiang E. O. Paton Welding Technology Research Institute, Hangzhou 311200, China*

modification of porous membranes in terms of membrane surface and pore wall modification.[24,25] In order to improve anti-fouling performance, nanomaterials (such as silica, graphene oxide, titanium dioxide, zinc oxide, *etc.*) have been mixed *in situ* into the polymer matrix to change the properties of the membrane.[26–29] Photolytic nanomaterials can further improve the anti-fouling performance of the membrane under light exposure. Fenton oxidation is intensively adaptable to pollutants and consumes low energy, so it is one of the most commonly utilized methods for deep treatment of organic pollutants in water.[30] Recently, the photo-Fenton method has been combined with membrane technology to improve the anti-fouling performance of membranes. For example, Wang *et al.*[31] reported a PVDF@$CuFe_2O_4$ membrane by incorporating $CuFe_2O_4$ into a PVDF membrane. Due to the high photo-Fenton activity, the membrane exhibits versatile anti-fouling properties against different types of dirt. Wu *et al.*[32] prepared TiO_2-PDA/PSF hybrid membranes *via* mixing and surface adhesion, which showed outstanding self-cleaning ability under ultraviolet irradiation. However, the compatibility of inorganic nanomaterials with soft polymer matrices is not satisfactory, giving rise to uneven aggregation and dispersion of nanoparticles, which will cause the separation performance of the membrane to be affected to a certain extent.[33]

In past studies, heterogeneous Fenton-like reaction is considered to be one of the powerful and economic advanced oxidation processes (AOPs) for the degradation of recalcitrant organics *via* hydroxyl radicals and/or superoxide radicals.[34,35] Among study that have been reported, the FeOOH is greatly promising as a viable photocatalyst because its Fe_3-μ_3-oxo cluster helps to purify water by producing hydroxyl radicals through photo-Fenton-like reactions.[36] Fenton oxidation has high adaptability to pollutants and low energy consumption, so Fenton technology is one of the most common methods of organic matter pollution in water. The photo-Fenton reaction uses Fe(III) for photolysis under light conditions to form Fe(II), which then continues to produce hydroxyl radicals through the photo-Fenton reaction. Thus, the cycle between Fe(III) and Fe(II) is effectively maintained, and the degradation rate of organic pollutants in water is accelerated. Xie *et al.*[37] used PVDF/NH_2-MIL-88B (Fe) (PVDF/NM88B) rich hydrophilic amino groups and high photo-Fenton activity to improve the self-cleaning ability of the hybrid membrane. Due to the hydrophilicity of NM88B and the high photo-Fenton activity, the PVDF/NM88B membrane exhibited excellent anti-fouling properties. Wang *et al.*[38] fabricated a negatively charged super hydrophilic membrane by depositing β-FeOOH nanorods on commercially available sulfonated polyolefin lithium-ion battery separators (LIBS), and the polyolefin surface-rich sulfonic acid groups provided sufficient binding sites for fixed β-FeOOH nanorods, using the β-FeOOH high-Fenton activity to impart the membrane efficient self-cleaning ability. Zhao *et al.*[39] adapted a polyphenol-metal-manipulated nano-hybridization strategy to make a novel super-wetting CNT@CS/TA-FeOOH nano-hybrid membrane with high permeability, oil resistance and self-cleaning properties. The methods of preparing photo Fenton membrane can be summarized into two kinds, one is to blend photo Fenton catalyst and polymer to prepare membrane, the other is to deposit a layer of photo Fenton catalyst on the surface of polymer membrane by *in situ* deposition. These two methods have a common defect, there is no chemical bond between the photo Fenton catalyst and the polymer. Due to the poor binding fastness between the photo Fenton catalyst and the polymer, the catalyst is easy to fall off in the process of use, resulting in the reduction of self-cleaning performance of the membrane. So based on the development of a new photo Fenton membrane preparation method.

Poly(ethylene-*alt*-maleic anhydride) (PEMA) has good hydrophilicity, not only can be dissolved in organic solvents, but also itself and its hydrolyzed products cannot be dissolved in water, widely used to regulate the hydrophilicity of polymer. In this work, we doped PEMA into the polyvinylidene fluoride (PVDF) to prepare PVDF/PEMA composite membrane *via* an *in situ* blending process, and then the PVDF/PEMA membrane was treated by acid and alkali to hydrolyze all maleic anhydride bonds into –COOH and $–COO^-$ group, thereby preparing a hydrophilic PVDF composite membrane. Last, on the basis of strong chelation between –COOH/$–COO^-$ groups and Fe(III), the β-FeOOH catalyst layer was generated on the surface by mineralization. The hydrophilic β-FeOOH endow the composite membrane with hydrophilicity, thus enhancing the anti-fouling performance. Meanwhile, the photo Fenton catalyst β-FeOOH to degrade oil pollutants through hydroxyl radicals and/or superoxide radicals, which improves the self-cleaning performance of the composite membrane. The catalyst and the substrate membrane are connected by chemical bonds, which has excellent stability. This membrane with superhydrophilicity and high self-cleaning properties has great application prospects in organic wastewater treatment.

2. Experimental part

2.1 Materials

Poly(vinylidene fluoride) (PVDF, Solvay 6010, $M_n = 500\,000$) was purchased from Solvay S.A. (America). Poly(ethylene-*alt*-maleic anhydride) (PEMA, $M_n = 50\,000$) was obtained from Vertellus (America). Polyvinylpyrrolidone (PVP, $M_n = 8000$), *N*,*N*-dimethylformamide (DMF), $FeCl_3 \cdot 6H_2O$, sodium dodecyl sulfate (SDS) and methylene blue (MB) were Shanghai Macklin Biochemical Co., Ltd (China). Ethanol, H_2O_2 (30%), 1,2-dichloroethane, hydrochloric acid (HCl, 36.0–38.0%) and NaOH was acquired from Hangzhou Gaojing Chemicals Co., Ltd.

2.2 Fabrication of PVDF hydrophilic composite membrane

The composite membrane was prepared by Nonsolvent Induce Phase Separation (NIPS). Firstly, PVDF (6 g), PEMA (0 g, 0.3 g, 0.6 g, 0.9 g, 1.2 g, 1.5 g) and PVP blended powder was dissolved in DMF solvent by magnetic stirring at 50 °C for 12 h, after standing overnight at 50 °C to obtain uniform cast solution (total mass of solution 50 g). The cast solution is immediately cast onto the glass substrate by a casting knife and immersed in a coagulation bath (deionized water), when the membrane was completely detached from the glass plate, the membrane was

immersed in deionized water for 24 h to completely remove PVP and DMF from the membrane. Then the prepared membranes were soaked in 0.1 mol L^{-1} HCl solution for 1 h and then soaked in 0.1 mol L^{-1} NaOH solution for 1 h. When the reaction was complete, the composite membrane was rinsed with deionized water and dried in a vacuum oven at 40 °C, named as membrane M0, M1, M2, M3, M4 and M5, respectively. According to the hydrophilic properties membranes, the membranes prepared under the optimal PEMA content were selected, and the following experiments were carried out (Fig. 1).

2.3 Fabrication of PVDF hydrophilic composite membranes loading β-FeOOH

A certain amount of $FeCl_3 \cdot 6H_2O$ and 50 mL HCl solution (pH = 2) was added into 100 mL deionized water forming a clear synthesis solution, the concentrations of Fe^{3+} are 0.025 mol L^{-1}, 0.05 mol L^{-1}, 0.075 mol L^{-1}, 0.1 mol L^{-1} and 0.125 mol L^{-1}, respectively. The above-mentioned washed membrane was immersed into the synthesis solution, slightly mechanically stirred at 50 °C for 24 h, then the modified membrane was rinsed with deionized water for 12 h to remove surface loose catalyst, and dried in a vacuum oven at 40 °C, named as membrane M@β-FeOOH(0.025), M@β-FeOOH(0.05), M@β-FeOOH(0.075), M@β-FeOOH(0.1) and M@β-FeOOH(0.125), respectively.

2.4 Oil-in-water emulsion separation experiment

In order to prepare a surfactant-stabilized oil-in-water emulsion, 1 g soybean oil and 0.2 g SDS were dissolved in 1 L deionized water, and then mixed liquor was stirred at 600 rpm for 2 h to obtain a stable oil-in-water emulsion. Emulsion droplet size was detected by a dynamic light scattering (DLS) (LB 550, HORIBA). Using the cross-flow filtration device, the oil–water separation is carried out under a constant pressure of 1 bar, the filtrate was collected after filtration, and the oil content before and after separation was detected by UV spectrophotometer at 220 nm, and the separation efficiency is calculated by the following eqn (1):

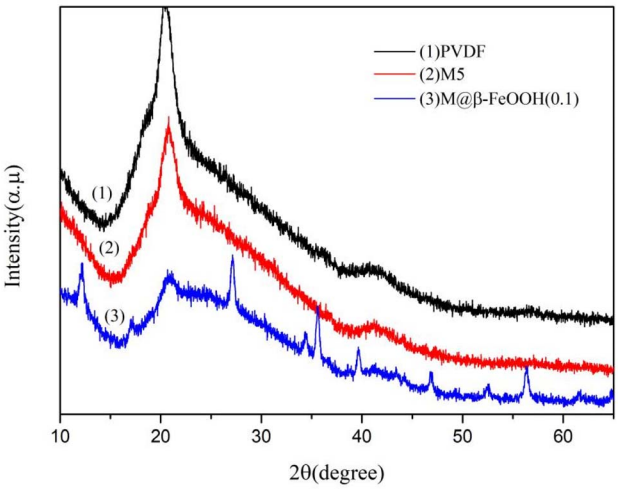

Fig. 2 XRD patterns of anatase PVDF, M5 and M@β-FeOOH(0.1).

$$R = \left(1 - \frac{C_f}{C_0}\right) \times 100\% \quad (1)$$

where C_f and C_0 represent the oil content of filtrate and raw emulsion measured by a UV spectrophotometer.

The flux is calculated by the following eqn (2):

$$J = \frac{V}{A \times \Delta t \times \Delta P} \quad (2)$$

where V (L) is the volume of permeable water, A (m^2) is the effective membrane area, Δt (h) is the separation time, and ΔP (bar) is the applied pressure.

To evaluate the self-cleaning performance of the membrane, calculate the flux recovery ratio (FRR). After the separation of oil-in-water emulsion, the composite membrane was simply cleaned with deionized water, and the membrane pure water permeation flux after cleaning was tested, and then the

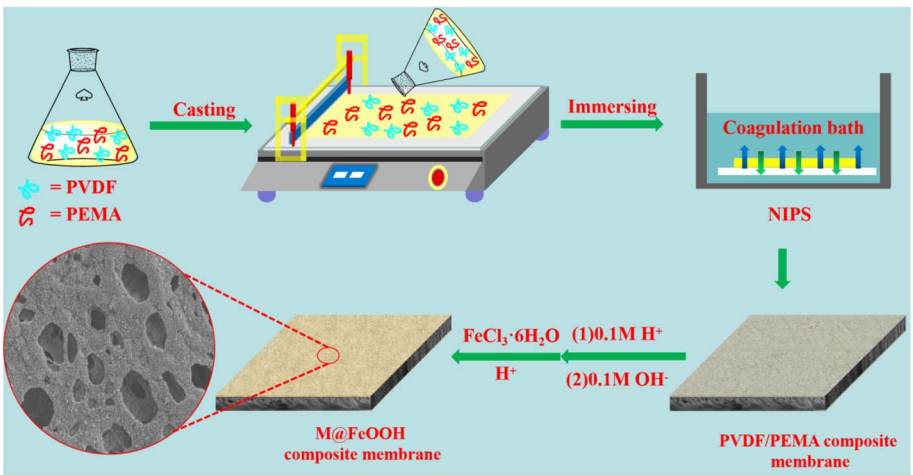

Fig. 1 A comprehensive description of the PVDF/@β-FeOOH membrane preparation process.

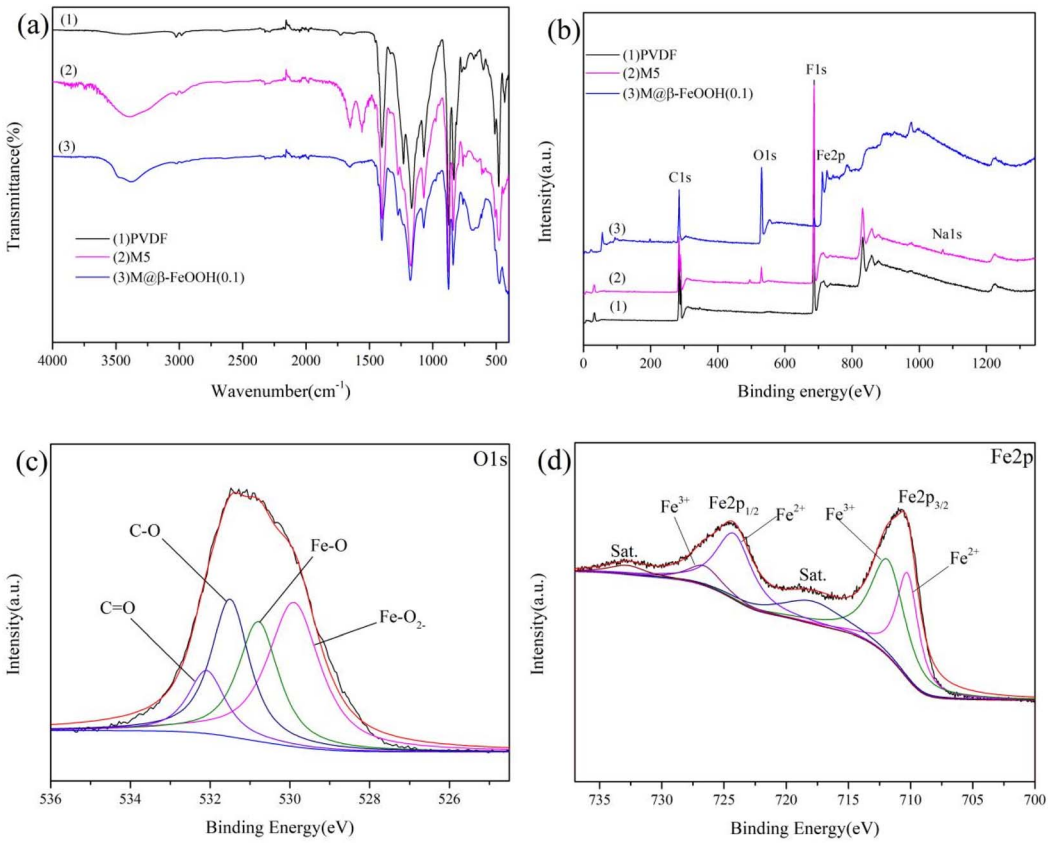

Fig. 3 (a) ATR-FTIR spectra of the membranes, (b) survey XPS spectra, (c) O1s and (d) Fe2p core-level XPS spectra of the M@β-FeOOH(0.1) membrane.

Table 1 Elemental composition of different membranes as determined by XPS

	Composition (at%)				
Membrane	C	F	O	Fe	Na
PVDF	57.11	42.89			
M5	54.05	41.22	4	—	0.72
M@β-FeOOH(0.1)	40.09	8.25	37.67	13.57	0.42

membrane was treated again by photo Fenton process and the membrane pure water permeation flux was tested. The FRR is calculated by the following eqn (3):

$$\mathrm{FRR} = \frac{J_F}{J_0} \times 100\% \quad (3)$$

where J_0 is the flux of pure water and J_F is the water flux of the membrane washed by the deionized water/photo-Fenton process.

2.5 Photo-Fenton catalytic capability tests

The photo-Fenton catalytic capability of the composite membrane was analysed by MB (initial concentration 10 mg L^{-1}) in dark and under UV irradiation, respectively. First, the membrane sample (diameter is 21 mm, thickness is 0.25 mm) was immersed in a beaker containing 50 mL dye solution, the solution was stirred in dark at room temperature to ensure adsorption/desorption equilibrium. Then, add 1 mL of H_2O_2 (30%) to the dye solution and the catalytic experiment was carried out under 250 W UV-lamp (main spectrum 365 nm). In the adsorption and catalytic processes, samples were taken at 1 h intervals the absorbance of each sample was measured by ultraviolet spectrophotometer at the maximum absorption wavelength of 664 nm.

2.6 Characterization

2.6.1 Instruments and methods. The surface morphology and cross-sectional morphology of the membrane was observed by JSM-5610LV field emission scanning electron microscope (JEOL, Japan). The Nicolet 5700 Fourier Transform Infrared Spectrometer (Thermo Electron Corporation, USA) determines the infrared spectrum of the membrane. X-ray diffraction is performed using an X-ray diffractometer. The mechanical properties of the membrane are tested with the YM065 power tester. The proportion of elements in the membrane was measured by K-Alpha X-ray photoelectron spectrometer. The absorption wavelength was determined with UH4150 UV-Visible NIR Spectrophotometer. The particle size of the oil–water emulsion is measured *via* Zetasizer Nano S Particle Size Analyzer (Malvern, Britain).

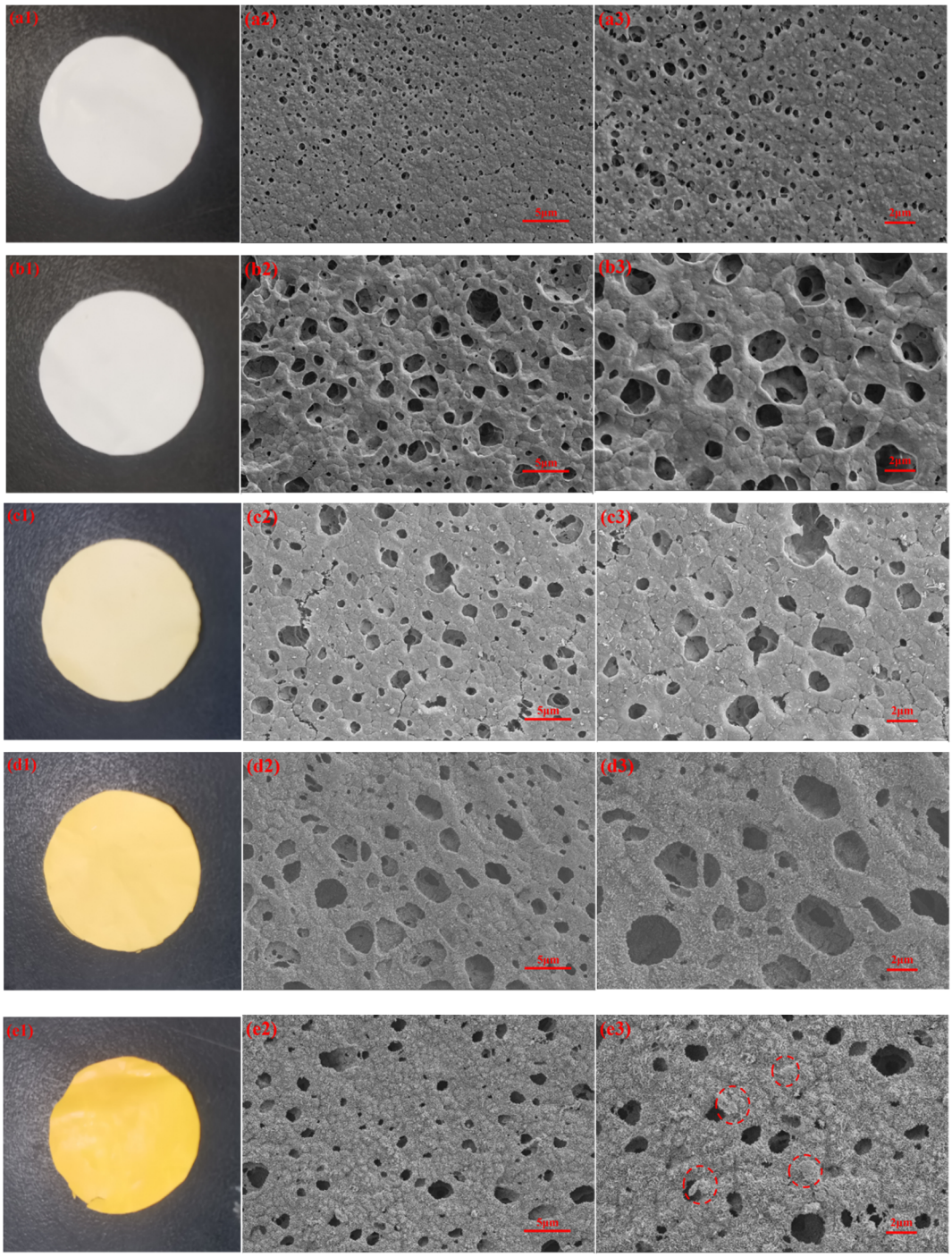

Fig. 4 The photographs and SEM images of PVDF (a), M4 (b), M@β-FeOOH(0.025) (c), M@β-FeOOH(0.1) (d) and M@β-FeOOH(0.125) (e).

3. Results and discussion

3.1 XRD analysis

The crystal structure of the prepared composite material was tested by XRD. As shown in Fig. 2, a diffraction peak at $2\theta = 20.8°$ was found, which constituted the typical XRD patterns of PVDF. As for M@β-FeOOH(0.1), other diffraction peaks at $2\theta = 12.18°$, 17.15°, 27.15°, 34.34°, 35.16°, 39.69°, 46.86°, 52.52°, 56.37° and 61.68° were attributed to (110), (200), (310), (400), (211), (301), (411), (600), (521) and (002) planes of β-FeOOH (JCPDS no. 34-1266).[40,41] The results show that β-FeOOH was successfully prepared on the surface of the composite membrane after mineralization.

3.2 Surface chemical structure analysis

The chemical composition of different membrane was analyzed by FTIR, as shown Fig. 3a. It can be seen that all the membranes

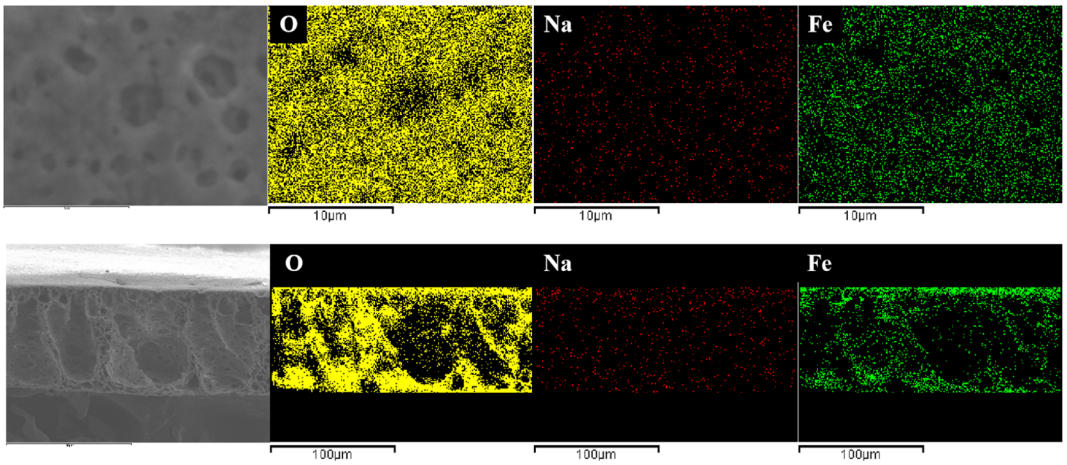

Fig. 5 The EDS mapping images of M@β-FeOOH(0.1) surface (a) and cross-section (b).

exhibited the peaks at 874 cm^{-1}, 1175 cm^{-1} and 1402 cm^{-1}, which were attributed to C–C, $–CF_2–$, $–CH_2–$, respectively. As for M5, two new characteristic peaks at 1558 cm^{-1} and 1652 cm^{-1} were found, which is ascribed to in $–COO^-$ bond resonance. Meanwhile, the peak intensity at 3000–3700 cm^{-1} became stronger, which attributed to the –OH.[42] Since the PVDF has a vibration peaks around 840 cm^{-1} belonging to Fe–O–Fe stretching vibrations are overlapped. Compared with the membrane, the vibration peaks of Fe–O–Fe stretching intensity are intensified, meanwhile, the new peaks at 688 cm^{-1} were attributed to the Fe–O stretching vibrations.[43] Additionally, it still has a strong –OH stretching vibration absorption peak at 3000–3700, which indicates a substantial increase in the hydroxyl groups from the β-FeOOH surface.

The surface composition and nature of the oxidation state was evaluated using XPS analysis. The survey spectra of PVDF, M5 and M@β-FeOOH(0.1) (Fig. 3b) displayed the same peaks of C1s and F1s. As for M5, the peak of O1s and Na1s were found due to the presence of –COOH and –COONa on the membrane surface. Compared with the PVDF and M5, the new peak was found at 710.8 eV, they are attributed to the Fe2p, which confirmed the presence of Fe element. Meanwhile, the peak intensity of O1s in the M@β-FeOOH(0.1) membrane is significantly enhanced. The elemental compositions of different membranes were shown in Table 1, which is consistent with the above XPS spectral results. To further verify the valence state of O and Fe element, a Gaussian fitting method was used to study the high-resolution XPS spectrum of O1s and Fe2p. For Fig. 3c, the O element fitting characteristic peaks of the M@β-FeOOH(0.1) membrane at 529.90, 530.79, 531.50 and 532.09 eV corresponding to the lattice oxygen of $Fe–O_2^-$, Fe–O, C–O and C═O, respectively.[44] Fig. 3d shows the Fe2p of the M@β-FeOOH(0.1) membrane high-resolution XPS spectra, it can been found that two satellites peaks at 717.86 eV and 732.76 eV are characteristic of the mixed valence Fe materials.[45] The fitting peaks at 710.24 eV and 724.20 eV corresponding to the Fe^{2+}, and the fitting peaks at 711.83 eV and 726.60 eV corresponding to the Fe^{3+}.[46] The above results are consistent with the XRD results, thus indicating that mixed-valent iron oxide (β-FeOOH) has been successfully loaded onto the PVDF membrane surface. The elemental compositions of different membranes were shown in Table 1, which is consistent with the above XPS spectral results.

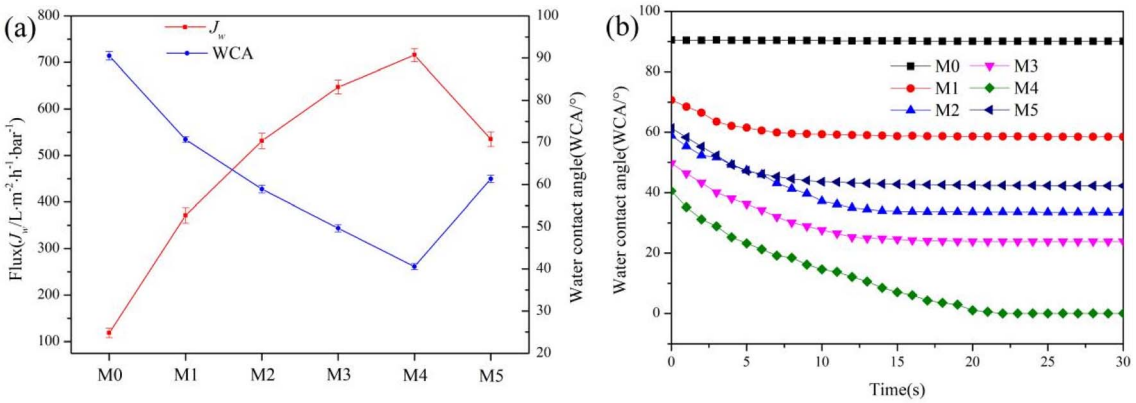

Fig. 6 The affection of PEMA content on hydrophilicity of composite membranes. (a) WCA and Flux, (b) dynamic WCA.

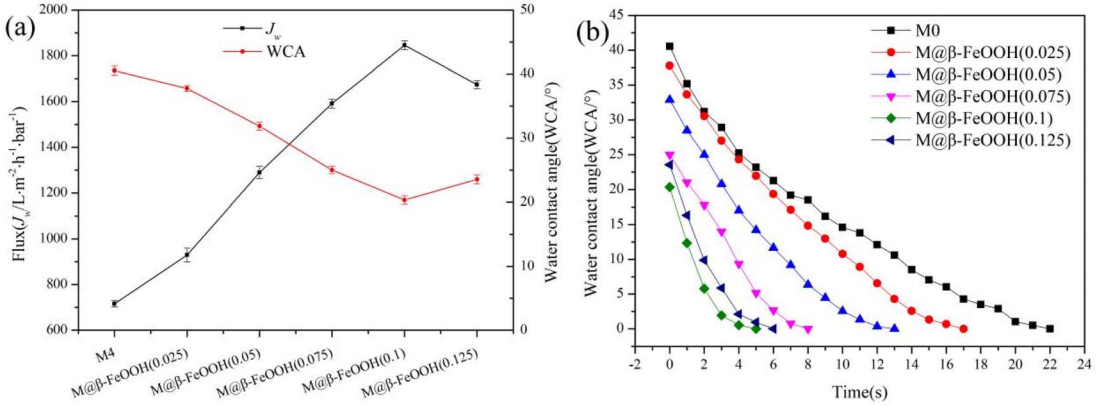

Fig. 7 The affection of $FeCl_3$ concentration on hydrophilicity of composite membranes.

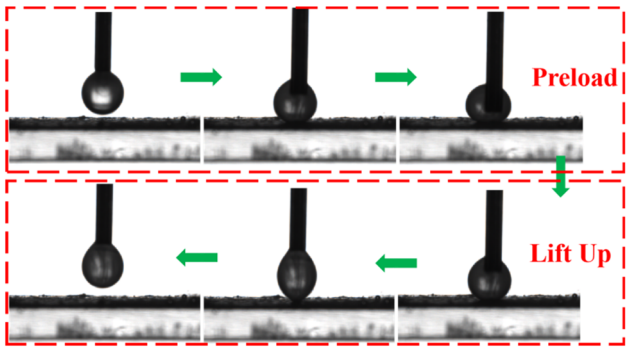

Fig. 8 Dynamic underwater oil-adhesion and underwater oil contact angle of the M@β-FeOOH(0.1) membrane (dichloromethane).

3.3 Morphologies of membrane

The surface morphologies of different membrane were investigated by SEM. Fig. 4 shows the optical photographs and corresponding SEM images of the membranes at different stages. It can be seen that the pristine PVDF and M5 membrane is white (Fig. 4a1 and b1). After mineralization, the membranes become yellow (Fig. 4c1–e1), which proves intuitively that β-FeOOH has mineralized on the membrane surface. Compared Fig. 4b2 and b3 with Fig. 4a2 and a3, it can be seen that with the addition of PEMA, the pore size of the blending membrane is larger than that of the PVDF membrane. The main reason is that PEMA is a hydrophilic polymer, and the presence of PEMA can accelerate the exchange rate of water from the coagulation bath to the casting solution, resulting in the pore size of the blending membrane become larger. Abundant particles can be observed on the surface of the M@β-FeOOH membranes (Fig. 4c2, c3–e2, e3). Furthermore, with the increase in the mass concentration of the $FeCl_3$ aqueous solution, the β-FeOOH particles becomes denser on the membrane surface and the pore size become small.

The EDS spectra was used to characterize the dispersion of O, Na and Fe elements in composite membrane. The EDS spectra of the surface and cross-section of M@β-FeOOH(0.1) is shown in Fig. 5. It can be found that O, Na and Fe elements were densely and uniformly distributed on the surface and cross-section of the composite membrane, which endows the composite membrane with excellent hydrophilicity and photocatalytic performance.

3.4 Surface water permeability and wettability of membranes

The hydrophilicity of the membrane is critical to the use of the membrane. The anhydride in PEMA has good hydrophilicity after hydrolysis, increasing the proportion of PEMA can improve the hydrophilicity of the composite membrane. In order to select the optimal ratio of PVDF to PEMA, the water contact angle and water flux test of PVDF/PEMA membranes with different PEMA content is performed, and the results are shown in Fig. 6. As shown in Fig. 6a, compared with the PVDF membrane, the WCA of composite membrane changed significantly. With the increase of the PEMA content from 0 to 20%, the values of WCA decrease from 90.5 ± 1.01° (M0) to 40.55 ± 0.72° (M4), and the values of J_w increase from 118.24 ± 10.18 (M0) to 715.72 ± 14.22 L m^{-2} h^{-1} bar^{-1} (M4). The main reason is that PEMA is a hydrophilic polymer, and a large number of carboxyl groups and carboxyl ions are formed after the hydrolysis of maleic anhydride in the membrane. With the increase of PEMA content, the content of hydrophilic groups in the membrane increases, resulting in the enhancement of membrane hydrophilicity. When the PEMA content is 25% (M5), the WCA slightly increased and J_w slightly decreased, it may be because the compatibility between PEMA and PVDF deteriorates, which makes PEMA not uniformly dispersed in the membrane, resulting in a decrease in the hydrophilicity of the membrane. The hydraulic permeability characterized by the dynamic water contact angle is vital to the hydrophilic membranes, and the results are shown in Fig. 6b. It can be seen that only the surface WCA of the M4 decreases to 0 after 22 s, and the WCA of the PVDF membrane basically does not change. The surface WCA of the membrane prepared under other PEMA content decreases slowly and then tends to be stable. Therefore, according to the hydrophilic properties of the membrane, the membrane prepared at 20% PEMA has the best performance.

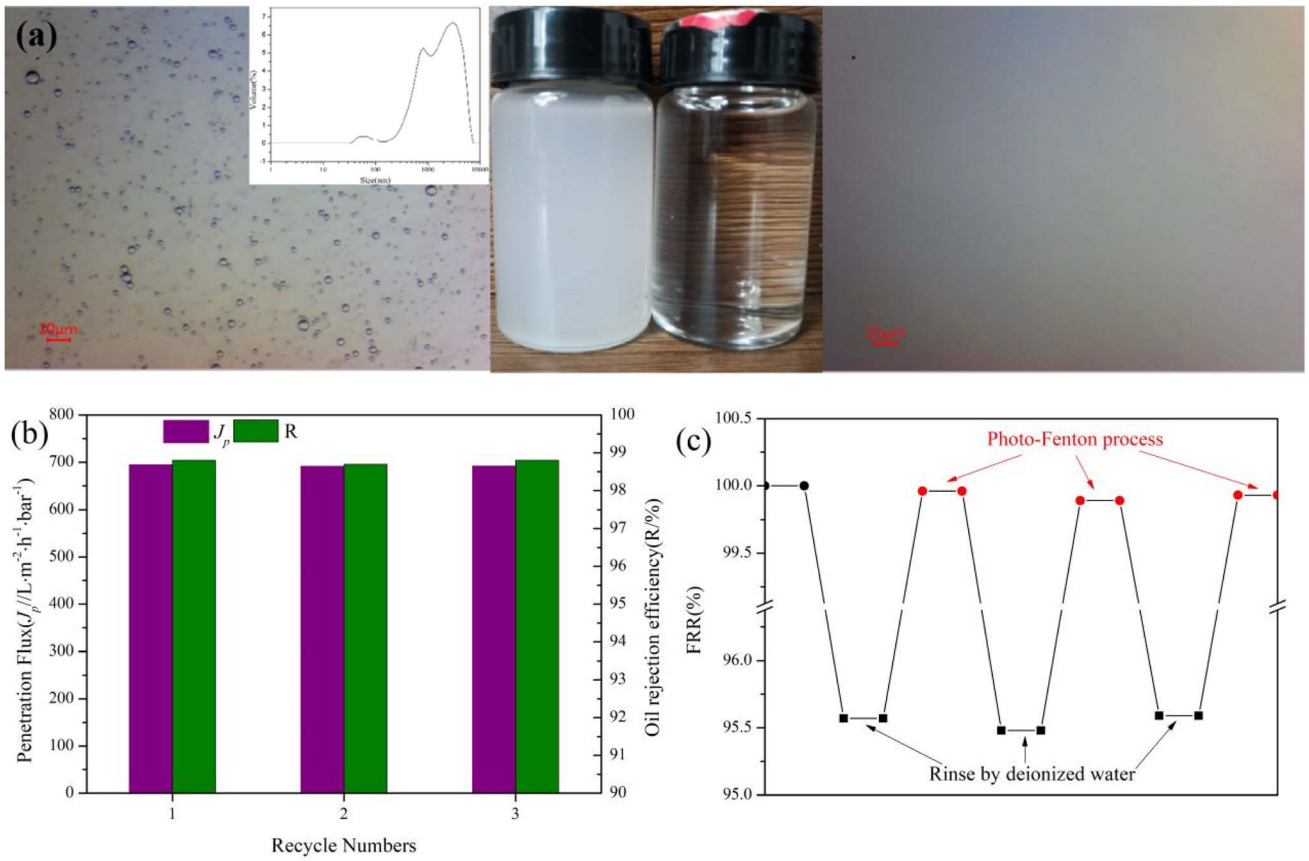

Fig. 9 (a) Optical micrographs and particle size distribution of emulsions before and after separation, (b) recyclability separation experiment of emulsion and (c) FRR of the membrane after rinsing under different conditions.

On the basis of the composite membrane prepared with 20% PEMA content, the affection of $FeCl_3$ concentration on the hydrophilicity of the composite membrane was further studied, and the results are shown in the Fig. 7. As shown Fig. 7a, with the increase of the $FeCl_3$ concentrations from 0 to 0.1 mol L^{-1}, the values of WCA decrease from 40.55 ± 0.72° (M4) to 20.34 ± 0.65° (M@β-FeOOH(0.1)), and the values of J_w increase from 715.72 ± 14.22 L m^{-2} h^{-1} bar^{-1} (M4) to 1845.65 ± 19.68 L m^{-2} h^{-1} bar^{-1} (M@β-FeOOH(0.1)). The main reason is that the number of hydrophilic groups on the membrane surface increases with the appearance of β-FeOOH particles. When $FeCl_3$ concentrations is too high, a large amount of β-FeOOH products accumulate on the membrane surface, which makes the membrane micropore blocked, the surface roughness is reduced, and the WCA on the membrane surface is increased, and the J_w is decreased. The membranes used in the subsequent experiments were prepared under these conditions. Meanwhile, the surface WCA of M@β-FeOOH(0.025), M@β-FeOOH(0.05), M@β-FeOOH(0.075), M@β-FeOOH(0.1) and M@β-FeOOH(0.125) can be reduced to 0° within 17 s, 13 s, 8 s, 5 s and 6 s, respectively (Fig. 7b). The results indicate that the hydrophilicity of the membrane can be further increased by the appearance of β-FeOOH particles.

3.5 Separation and anti-fouling performance

The underwater superoleophobicity of the membrane determines the separation performance of the membrane during oil–water separation, which is determined by its underwater dynamic viscous oil performance and underwater oil contact angle (UOCA). Fig. 8 investigates the underwater dynamic viscous oil properties of the M@β-FeOOH(0.1) membrane and the UOCA. It can be seen from the Fig. 8 that when the dichloromethane droplets were first forced to fully contact the surface of the M@β-FeOOH(0.1) membrane under water and then lifted up, the oil droplets remained almost spherical, and there was no visible residue on the membrane surface. Meanwhile, the UOCA of the M@β-FeOOH(0.1) membrane to dichloromethane is 155.10°, indicating that the M@β-FeOOH(0.1) membrane has excellent anti-oil adhesion and/underwater superoleophobic properties under water.

To evaluate the oil-in-water emulsion separation performance of composite membrane, the separation experiment of soybean oil-in-water emulsion was carried, the result was shown in Fig. 9. Fig. 9a shows the optical microscope images before and after separation of the oil-in-water emulsion. It can be seen that the emulsion before separation is milky white, and the dense oil droplets can be clearly observed in the optical micrographs, the filtrate after separation is clear and no oil

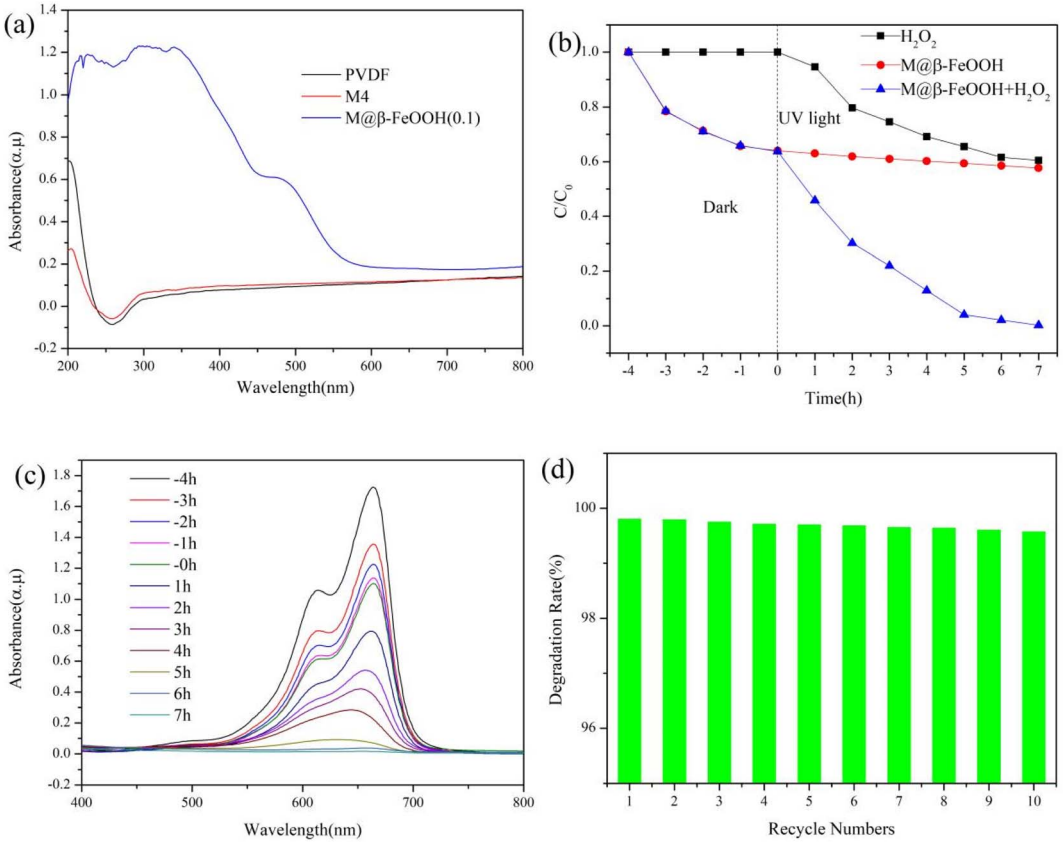

Fig. 10 (a) UV-vis diffuse reflection spectra of the PVDF, PEMA, M4 and M@β-FeOOH(0.1), (b) the dynamic curve of the H_2O_2 and photo-Fenton catalytic degradation for the removal of MB, (c) UV-vis adsorption spectra of the MB solution over photo-Fenton catalytic degradation process, (d) photo-Fenton catalytic degradation performance of the M@β-FeOOH(0.1) for MB (b) during 10 cycles.

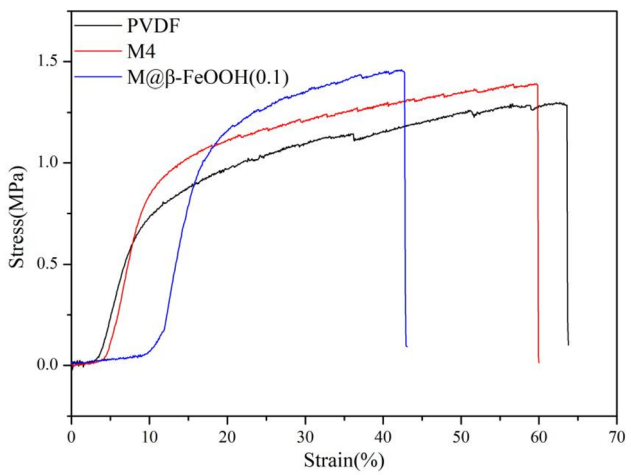

Fig. 11 The stress–strain curves of the membranes.

droplets are observed in the optical micrographs, indicating the high efficiency of the M@β-FeOOH(0.1) membrane for oil-in-water emulsion separation. As shown Fig. 8b, it can be found that the separation efficiency reached 98.8% and penetration flux reached 694.56 L m^{-2} h^{-1} bar^{-1}. Meanwhile, in order to study the reusable performance of the composite membrane in oil–water separation, three times of soybean oil-in-water emulsion filtration experiments were performed on the prepared composite membrane, and the results were shown in Fig. 9b. The M@β-FeOOH(0.1) membrane can achieve a separation efficiency of more than 98.7% in three cycles of soybean oil-in-water emulsion, and has a high permeation flux. After each separation experiment, the composite membrane was washed with deionized water and photo-Fenton process, the FRR of the composite membrane after deionized water washing and photo-Fenton process were tested respectively, the results were shown in Fig. 9c. It can be seen that after oil/water separation, the FRR of the composite membrane reaches 95.57% after simple deionized water washing, while the FRR of the composite membrane reaches 99.93% after photo-Fenton process, indicating that photo-Fenton cleaning can effectively remove oil stains on the membrane surface. After three cycles, the FRR of the composite membrane still reached 99.9%, indicating that the membrane has excellent cleaning ability. The results show that the membrane has good recyclability and self-cleaning performance.

3.6 Photo-Fenton catalytic capability

The optical property of the membrane was analyzed by ultraviolet-visible infrared spectroscopy (UV-vis DRS). As shown

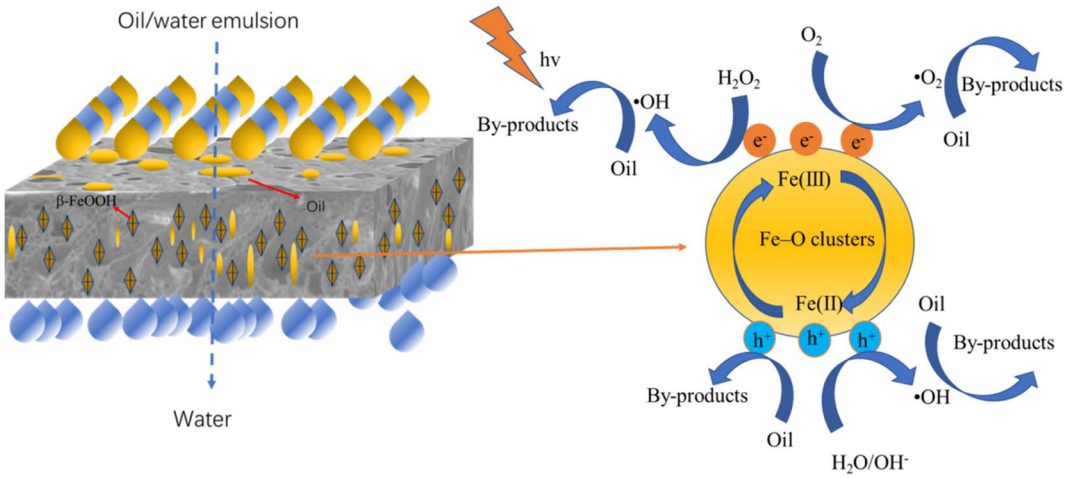

Fig. 12 Mechanisms of self-cleaning for M@β-FeOOH(0.1) membrane.

in Fig. 10a, compared with PVDF and M4, the M@β-FeOOH(0.1) membrane has a stronger absorption peak at 302–600 nm. These results show that the prepared composite membrane has a high utilization rate of light energy, which is conducive for improving the photo-Fenton catalytic activity. In this experiment, MB was selected as a simulated organic pollutant because of its hazards and prevalence in the aquatic environment. The photo-Fenton activity of the M@β-FeOOH(0.1) membrane is estimated based on the degradation of MB under UV light irradiation. As shown Fig. 10b, when only H_2O_2 was added to the MB solution, the MB degradation rate was 39.5%. When only M@β-FeOOH(0.1) was added to the MB solution, the adsorption experiment was carried out in the dark condition, and the UV-light was carried out after equilibrium, and it can been found that the dye concentration did not change much. When the M@β-FeOOH(0.1) and H_2O_2 was added to the MB solution, the MB degradation rate was as high as 99.8% at the same UV light time. The changes in the UV-vis adsorption spectra for the MB solution are shown in Fig. 10c. The MB solution shows a strong absorbance at 664 nm, and the absorbance almost disappears after 7 h. These results indicate that the conjugated chromophore structure was destroyed and the MB molecules were completely degraded into small organic/inorganic molecular or/and ionic products, as demonstrated by a previous research on the degradation pathway of MB in β-FeOOH@GO catalyzed photo-Fenton-like system.[47] The reusability of catalytic membrane plays an important role in practical applications, as this study experiments on the reusability of the membrane and the results are shown in Fig. 10d. After the first photocatalytic dye degradation experiment, the M@β-FeOOH(0.1) membrane was washed with deionized water, and then placed in fresh dye solution to repeat the adsorption degradation experiment. It can be seen from Fig. 8d that the degradation rate of the M@β-FeOOH(0.1) decreases slightly after running 10 times, but the M@β-FeOOH(0.1) exhibited great recyclability with 99.5% degradation ratio for RhB, demonstrating that the photo-Fenton catalytic performance of the M@β-FeOOH(0.1) is relatively stable and can be recycled.

3.7 Mechanical properties of the membrane

The application of the membrane also has a certain relationship with its mechanical properties. Excellent mechanical properties will directly affect the application field of the membrane. Therefore, the mechanical properties of the membrane are evaluated by testing the stress–strain curve of the membrane, the result is shown in Fig. 11. The tensile strength of the composite membrane is higher than that of the PVDF and M4 membrane. On the one hand, due to the hydrogen bonding between the rich –COOH and $–COO^-$ groups and fluorine groups on the PVDF chain may contribute to the improvement of mechanical property. On the other hand, after in mineralization of β-FeOOH, a large number of β-FeOOH particles appear on the membrane surface, which leads to the increase of membrane surface roughness, so that the tensile strength of composite membrane further increase. In conclusion, the prepared composite membrane has good mechanical property and has potential application value in the field of sewage treatment.

3.8 Mechanism of photo-Fenton self-cleaning

During the oil-in-water separation experiment, the water will pass through the composite membrane, and the oil will remain in the surface layer or pore of the composite membrane, causing membrane pollution. The contaminated composite membrane is self-cleaning through photo-Fenton, a possible mechanism was proposed and displayed in Fig. 12. The M@β-FeOOH(0.1) membrane has Fe–O clusters, and can be activated and produce photo-induced carriers. Photoelectrons (e^-) can promote the decomposition of H_2O_2 to produce $·OH$[48] Moreover, some e-may be captured by O_2, further forming $·O_2^-$.[49] Therefore, the oil on the membrane can be decomposed by the strong oxidation of $·OH$ and $·O_2^-$ oxidation. Meanwhile, the remaining h^+ can directly oxidize the oil deposited on the surface of the composite membrane. H_2O_2 reacts with Fe(III) in the M@β-FeOOH(0.1) membrane to form Fe(II), Fe(II) further promote the decomposition of H_2O_2, and generates $·OH$ by the

light Fenton reaction. At the same time, the β-FeOOH is oxidized to its initial state, thus producing a large amount of ·OH in the cyclic reaction. Thus, even in the absence of light, the oil deposited in the membrane pores can be oxidized and decomposed. The strong photo-Fenton self-cleaning capability makes the composite membrane have broad application prospects in wastewater remediation.

4. Conclusion

In summary, a composite membrane with self-cleaning properties was prepared by using phase conversion method after blending PEMA with PVDF, and then Fe^{3+} was mineralized into β-FeOOH particles and deposited on the PVDF/PEMA composite membrane. A large number of –COOH/COO^- and β-FeOOH particles on the membrane surface make the composite membrane have strong hydrophilic properties (WCA = 20.34°) and underwater superoleophobicity (UOCA = 155.10°). Moreover, the composite membrane has high separation efficiency (98.8%) and penetration flux (694.56 L m^{-2} h^{-1} bar^{-1}) for soybean oil-in-water emulsion. Furthermore, the β-FeOOH with the robust photo-Fenton catalytic activity could remove oil foulants adsorbed onto the membrane surface by catalytic degradation, which granted the M@β-FeOOH(0.1) membrane with better self-cleaning performance and flux recovery (over 99.9%), and the β-FeOOH is chemically bonded to the as-prepared membrane, which makes the as-prepared membrane have good reusability. The present work provides a useful way to deal with membrane fouling in oil/water emulsion separation.

Conflicts of interest

The authors declare no competing financial interest.

Acknowledgements

We gratefully thank the National Key Research and Development Program of China (grant no. 2021YFB3801502) and the Fund for the Research Start-up Fund project of Zhejiang Sci-Tech University (grant no. 22202003-Y) for support of this program.

References

1 L. Qin, D. L. Huang, P. Xu, G. M. Zeng, C. Lei and Y. K. Fu, *In situ* deposition of gold nanoparticles onto polydopamine-decorated g-C_3N_4 for highly efficient reduction of nitroaromatics in environmental water purification, *J. Colloid Interface Sci.*, 2019, **534**, 357–369.

2 C. C. Li, X. Y. Chen, J. Luo, F. Wang, G. J. Liu, H. L. Zhu and Y. H. Guo, PVDF grafted gallic acid to enhance the hydrophilicity and antibacterial properties of PVDF composite membrane, *Sep. Purif. Technol.*, 2021, **259**, 118127.

3 Z. L. Li, J. Y. Chen and Y. Y. Ge, Removal of lead ion and oil droplet from aqueous solution by lignin-grafted carbon nanotubes, *Chem. Eng. J.*, 2017, **308**, 809–817.

4 C. C. Li, Z. H. He, F. Wang, H. L. Zhu, Y. H. Guo and M. Y. Chen, Laccase-catalyzed homo-polymer of GAL and cross-linking with PEI to enhance hydrophilicity and anti-fouling property of PTFE flat membrane, *Prog. Org. Coat.*, 2019, **132**, 429–439.

5 B. Song, M. Chen, S. J. Ye, P. Xu and G. M. Zeng, Effects of multi-walled carbon nanotubes on metabolic function of the microbial community in riverine sediment contaminated with phenanthrene, *Carbon*, 2019, **144**, 1–7.

6 Y. F. Long, Y. Q. Shen, H. F. Tian, Y. X. Yang, H. Feng and J. Li, Superwettable Coprinus comatus coated membranes used toward the controllable separation of emulsified oil/water mixtures, *J. Membr. Sci.*, 2018, **565**, 85–94.

7 Y. Liao, M. Tian and R. Wang, A high-performance and robust membrane with switchable super-wettability for oil/water separation under ultralow pressure, *J. Membr. Sci.*, 2017, **543**, 123–132.

8 A. T. Xie, J. D. Dai, C. H. Ma, J. Y. Cui and Y. Y. Chen, Construction of caterpillar-like cobalt-nickel hydroxide/carbon cloth hierarchical architecture with reversible wettability towards on-demand oil-water separation, *Appl. Surf. Sci.*, 2018, **462**, 659–668.

9 Z. Xu, D. Y. Jiang, Z. B. Wei, J. Chen and J. F. Jing, Fabrication of superhydrophobic nano-aluminum films on stainless steel meshes by electrophoretic deposition for oil-water separation, *Appl. Surf. Sci.*, 2018, **427**, 253–261.

10 J. Y. Cui, Z. P. Zhou, A. T. Xie, Q. Q. Wang and S. W. Liu, Facile preparation of grass-like structured NiCo-LDH/PVDF composite membrane for efficient oil–water emulsion separation, *J. Membr. Sci.*, 2019, **573**, 226–233.

11 X. Yang, Y. He, G. Y. Zeng, X. Chen, H. Shi and D. Y. Qing, Bio-inspired method for preparation of multiwall carbon nanotubes decorated superhydrophilic poly(vinylidene fluoride) membrane for oil/water emulsion separation, *Chem. Eng. J.*, 2017, **321**, 245–256.

12 C. J. Wei, F. Y. Dai, L. G. Lin, Z. H. An, Y. He and X. Chen, Simplified and robust adhesive-free superhydrophobic SiO_2-decorated PVDF membranes for efficient oil/water separation, *J. Membr. Sci.*, 2018, **555**, 220–228.

13 Y. H. Dou, D. L. Tian, Z. Q. Sun, Q. N. Liu, N. Zhang and J. H. Kim, Fish Gill Inspired Crossflow for Efficient and Continuous Collection of Spilled Oil, *ACS Nano*, 2017, **11**(3), 2477–2485.

14 C. C. Li, J. Q. Wang, Y. Y. Luo, F. Wang, H. L. Zhu and Y. H. Guo, One-bath two step method combined surface micro/nanostructures treatment to enhance anti-fouling and antibacterial property of PTFE flat membrane, *J. Taiwan Inst. Chem. Eng.*, 2019, **96**, 639–651.

15 J. Y. Cui, A. T. Xie, S. Zhou, S. W. Liu, Q. Q. Wang and Y. L. Wu, Development of composite membranes with irregular rod-like structure *via* atom transfer radical polymerization for efficient oil-water emulsion separation, *J. Colloid Interface Sci.*, 2019, **533**, 278–286.

16 C. C. Li, Y. L. Luo, H. Y. Zhang, Q. Q. Liao, D. Xu, J. Q. Wang, G. J. Liu, H. L. Zhu and Y. H. Guo, Carboxymethyl cellulose and cross-linking with polyethyleneimine to enhance hydrophilicity and anti-fouling property of

polytetrafluoroethylene flat membrane, *Desalin. Water Treat.*, 2022, **270**, 12–24.

17 J. Y. Cui, Z. P. Zhou, A. T. Xie, M. J. Meng, Y. H. Cui and S. W. Liu, Bio-inspired fabrication of superhydrophilic nanocomposite membrane based on surface modification of SiO_2 anchored by polydopamine towards effective oil-water emulsions separation, *Sep. Purif. Technol.*, 2019, **209**, 434–442.

18 J. Q. Zhang, X. L. Pan, Q. Z. Xue, D. L. He, L. Zhu and Q. K. Guo, anti-fouling hydrolyzed polyacrylonitrile/graphene oxide membrane with spindle-knotted structure for highly effective separation of oil-water emulsion, *J. Membr. Sci.*, 2017, **532**, 38–46.

19 J. Q. Zhang, Q. Z. Xue, X. L. Pan, Y. K. Jin, W. B. Lu, D. G. Ding and Q. K. Guo, Graphene oxide/polyacrylonitrile fiber hierarchical-structured membrane for ultra-fast microfiltration of oil-water emulsion, *Chem. Eng. J.*, 2017, **307**, 643–649.

20 J. H. Jhaveri and Z. V. P. Murthy, A comprehensive review on anti-fouling nanocomposite membranes for pressure driven membrane separation processes, *Desalination*, 2016, **379**, 137–154.

21 Y. F. Mu, K. Zhu, J. S. Luan, S. L. Zhang, C. Y. Zhang, R. Q. Na and Y. C. Yang, Fabrication of hybrid ultrafiltration membranes with improved water separation properties by incorporating environmentally friendly taurine modified hydroxyapatite nanotubes, *J. Membr. Sci.*, 2019, **577**, 274–284.

22 N. Nasrollahi, S. Aber, V. Vatanpour and N. M. Mahmoodi, Development of hydrophilic microporous PES ultrafiltration membrane containing CuO nanoparticles with improved anti-fouling and separation performance, *Mater. Chem. Phys.*, 2019, **222**, 338–350.

23 Q. Li, Z. P. Liao, X. F. Fang, D. P. Wang, J. Xie, X. Y. Sun, L. J. Wang and J. S. Li, Tannic acid-polyethyleneimine crosslinked loose nanofiltration membrane for dye/salt mixture separation, *J. Membr. Sci.*, 2019, **584**, 324–332.

24 X. T. Zhao, N. Jia, L. J. Cheng, L. F. Cheng and C. J. Gao, Dopamine-induced biomimetic mineralization for *in situ* developing anti-fouling hybrid membrane, *J. Membr. Sci.*, 2018, **560**, 47–57.

25 X. T. Zhao, N. Jia, L. J. Cheng, L. F. Liu and C. J. Gao, Metal-polyphenol coordination networks: towards engineering of anti-fouling hybrid membranes *via in situ* assembly, *J. Membr. Sci.*, 2018, **563**, 435–446.

26 Z. X. Liu, Z. M. Mi, S. Z. Jin, C. B. Wang, D. M. Wang and X. G. Zhao, The influence of sulfonated hyperbranched polyethersulfone-modified halloysite nanotubes on the compatibility and water separation performance of polyethersulfone hybrid ultrafiltration membranes, *J. Membr. Sci.*, 2018, **557**, 13–23.

27 N. Nasrollahi, V. Vatanpour, S. Aber and N. M. Mahmoodi, Preparation and characterization of a novel polyethersulfone (PES) ultrafiltration membrane modified with a CuO/ZnO nanocomposite to improve permeability and anti-fouling properties, *Sep. Purif. Technol.*, 2018, **192**, 369–382.

28 S. Y. Ding, L. L. Zhang, Y. Li and L. A. Hou, Fabrication of a novel polyvinylidene fluoride membrane *via* binding SiO_2 nanoparticles and a copper ferrocyanide layer onto a membrane surface for selective removal of cesium, *J. Hazard. Mater.*, 2019, **368**, 292–299.

29 L. Zhang, Y. Lu, Y. L. Liu, M. Li, H. Y. Zhao and L. A. Hou, High flux MWCNTs-interlinked GO hybrid membranes survived in cross-flow filtration for the treatment of strontium-containing wastewater, *J. Hazard. Mater.*, 2016, **320**, 187–193.

30 F. T. Chen, X. X. Shi, X. B. Chen and W. X. Chen, An iron (II) phthalocyanine/poly(vinylidene fluoride) composite membrane with anti-fouling property and catalytic self-cleaning function for high-efficiency oil/water separation, *J. Membr. Sci.*, 2018, **552**, 295–304.

31 T. Wang, Z. Y. Wang, P. L. Wang and Y. Y. Tang, An integration of photo-Fenton and membrane process for water treatment by a PVDF@$CuFe_2O_4$ catalytic membrane, *J. Membr. Sci.*, 2019, **572**, 419–427.

32 H. Q. Wu, Y. J. Liu, L. Mao, C. H. Jiang, J. M. Ang and X. H. Lu, Doping polysulfone ultrafiltration membrane with TiO_2-PDA nanohybrid for simultaneous self-cleaning and self-protection, *J. Membr. Sci.*, 2017, **532**, 20–29.

33 V. T. Hoang and S. Kaliaguine, Predictive models for mixed-matrix membrane performance: a review, *Chem. Rev.*, 2013, **113**(7), 4980–5028.

34 O. Gokkus, F. Coskun, M. Kocaoglu and Y. S. Yidiz, Determination of optimum conditions for color and COD removal of Reactive Blue 19 by Fenton oxidation process, *Desalin. Water Treat.*, 2014, **52**, 31–33.

35 O. Gokkus and M. Oguz, Investigation of color and COD removal by Fenton reagent from aqueous solutions containing acid and reactive dyestuffs, *Desalin. Water Treat.*, 2011, **26**, 1–3.

36 H. Z. Sun, B. B. Tang and P. Y. Wu, Hydrophilic hollow zeolitic imidazolate framework-8 modified ultrafiltration membranes with significantly enhanced water separation properties, *J. Membr. Sci.*, 2018, **551**, 283–293.

37 A. T. Xie, J. Y. Cui, J. Yang, Y. Y. Chen, J. H. Lang, C. X. Li, Y. S. Yan and J. D. Dai, Photo-Fenton self-cleaning PVDF/NH_2-MIL-88B(Fe) membranes towards highly-efficient oil/water emulsion separation, *J. Membr. Sci.*, 2020, **595**, 117499.

38 M. Wang, Z. W. Xu, Y. L. Guo, Y. F. Hou, P. Li and Q. J. Niu, Engineering a superwettable polyolefin membrane for highly efficient oil/water separation with excellent self-cleaning and photo-catalysis degradation property, *J. Membr. Sci.*, 2020, **611**, 118409.

39 X. T. Zhao, L. J. Cheng, N. Jia, R. X. Wang, L. F. Liu and C. J. Gao, Polyphenol-metal manipulated nanohybridization of CNT membranes with FeOOH nanorods for high-flux, anti-fouling and self-cleaning oil/water separation, *J. Membr. Sci.*, 2020, **600**, 117857.

40 N. Liu, R. X. Qu, Y. Chen, Y. N. Cao, W. F. Zhang, X. Lin, Y. Wei, L. Feng and L. Jiang, *In situ* dual-functional water purification with simultaneous oil removal and visible light catalysis, *Nanoscale*, 2016, **8**, 18558–18564.

41 L. F. Mei, L. B. Liao, Z. S. Wang and C. C. Xu, Interactions between Phosphoric/Tannic Acid and Different Forms of FeOOH, *Adv. Mater. Sci. Eng.*, 2015, **2015**, 250836.

42 J. E. Chen, X. R. Meng, Y. R. Tian and X. D. Wang, Fabrication of a superhydrophilic PVDF-g-PAA@FeOOH ultrafiltration membrane with visible light photo-fenton self-cleaning performance, *J. Membr. Sci.*, 2020, **616**, 118587.

43 T. S. Jiang, L. Yan, L. Zhang, Y. Y. Li, Q. Zhao and H. B. Yin, Fabrication of a novel graphene oxide/β-FeOOH composite and its adsorption behavior for copper ions from aqueous solution, *Dalton Trans.*, 2015, **44**, 10448–10456.

44 Y. Y. Liu, X. M. Liu, Y. P. Zhao and D. D. Dionysiou, Aligned alpha-FeOOH nanorods anchored on a graphene oxide-carbon nanotubes aerogel can serve as an effective Fenton-like oxidation catalyst, *Appl. Catal., B*, 2017, **213**, 74–86.

45 T. Fujii, F. M. F. D. Groot, G. A. Sawatzky, F. C. Voogt, T. Hibma and K. Okada, *In situ* XPS analysis of various iron oxide films grown by NO_2-assisted molecular-beam epitaxy, *Phys. Rev. B: Condens. Matter Mater. Phys.*, 1999, **59**, 3195.

46 L. Y. Zhang, H. Li, B. W. Yang, N. Han, Z. T. Zhang and Y. Zhou, Promote the electrocatalysis activity of amorphous FeOOH to oxygen evolution reaction by coupling with ZnO nanorod array, *J. Solid State Electrochem.*, 2020, **24**, 905–914.

47 S. S. Su, Y. Y. Liu, X. M. Liu, W. Jin and Y. P. Zhao, Transformation pathway and degradation mechanism of methylene blue through beta-FeOOH@GO catalyzed photo-Fenton-like system, *Chemosphere*, 2019, **218**, 83–92.

48 C. Gao, S. Chen, X. Quan, H. T. Yu and Y. B. Zhang, Enhanced Fenton-like catalysis by iron-based metal organic frameworks for degradation of organic pollutants, *J. Catal.*, 2017, **356**, 125–132.

49 H. N. Che, C. B. Liu, W. Hu, H. Hu, J. Q. Li, J. Y. Dou and W. D. Shi, NGQD active sites as effective collectors of charge carriers for improving the photocatalytic performance of Z-scheme g-C_3N_4/Bi_2WO_6 heterojunctions, *Catal. Sci. Technol.*, 2018, **8**(2), 622–631.